EurJIC
European Journal of Inorganic Chemistry

Research Article
doi.org/10.1002/ejic.202300358

Chemistry Europe
European Chemical Societies Publishing

www.eurjic.org

Color Tunable Emission and Oxygen Sensing from a Discrete Europium–Pyrene Assembly

Alex T. O'Neil,[a] Jade Pope,[a] John A. Harrison,[a] and Jonathan A. Kitchen*[a]

We report the synthesis of a new pyrene, dipicolinic acid-based ligand ($\mathbf{L_1H}$) and its corresponding multi-emissive and multi-functional europium complex [Eu($\mathbf{L_1}$)$_3$] that is capable of single component color switchable emission from red to blue and also white. At high concentration (10 mM) the single component system results in near pure white emission (CIE coordinates x,y = 0.329, 0.324). Furthermore, the system showed ratiometric oxygen sensing with oxygen significantly quenching the pyrene centered emission but not the Eu^{3+} emission, resulting in an overall emission color change from blue to red on increasing oxygen content.

Introduction

Multi-emissive molecular systems are high value targets in the advanced materials sector because of the wide array of applications to which they can be tuned. These include ratiometric sensors (for oxygen,[1] temperature,[2] or different analytes),[3] molecular barcodes[4] or logic gates,[5] multicolor cell imaging,[6] and single component white light generation.[7] There are many approaches to developing multi-emissive systems, including from solely organic materials[8] or by combining emission from metals and organic components (as discrete complexes,[7a] coordination polymers[4] or metal organic frameworks).[3a] The latter approach allows for multi-emissive systems, in which the luminophore emissions can be distinct from one another, allowing for multi-emissive systems where the luminophores respond independently to changes in their environment. Such independent emission is highly desired as it allows for controlled color tunable emission where the emission output can be tuned for a desired application. For example, white emission by fine tuning emission intensities;[7b,d] self-calibrating and ratiometric sensors where one luminophore is changed by an analyte while the other is not[1b] and/or fluorescent chameleon sensors where changes in luminophore intensity result in overall emission color-profile changes.[2b,9] Trivalent lanthanide ions (Ln^{3+}) are particularly good candidates for inclusion into multi-emissive systems as they are well known for their unique photophysical properties. Ln^{3+} ions emit over a large portion of the electronic spectrum (including in the UV, visible and NIR regions), have very distinct narrow line like emissions, are emissive in both solution and solid states and can be relatively unaffected by their external environment with limited vibronic relaxation effects.[10] However, due to the forbidden nature of the *f-f* transition, direct excitation of the Ln^{3+} excited states is relatively inefficient, and it is more common to use an organic ligand to indirectly populate these excited states (the "antenna" effect).[10] In our present study a single component Ln^{3+} coordination complex approach has been utilized to generate a multi-emissive system where an organic emitting chromophore is incorporated in the ligand structure (Scheme 1). Multi-emission from a discrete single component complex is ideal as it allows for color-tunability as well as solution processing into material coatings using methods such as spin coating,[2b] Langmuir Blodgett[11] and RASS.[12] When designing multi-emissive coordination complexes careful consideration must be given to both the metal (in this study, appropriate binding site and antenna ability for Eu^{3+}) and the organic chromophore. $\mathbf{L_1H}$ has been designed with the blue emitting pyrene moiety as the organic chromophore intentionally positioned distant from the 6-carbamoylpyridine-2-carboxylic acid (PDC) Ln^{3+} binding site. PDC has been shown to form 1:3 M:L coordination complexes with Ln^{3+} and is an effective antenna for a range of visibly emitting Ln^{3+}, including the red emissive Eu^{3+} which is utilized in this study.[11a] Pyrene exhibits blue monomer emission at ~370–430 nm and under certain conditions can exhibit dual emission with a secondary cyan colored excimer emission at ~490 nm.[13] Pyrene is relatively uncommon in combination with Ln^{3+}, yet pyrene has been found to be an effective antenna for visibly emissive Ln^{3+},[14] and NIR emitting Ln^{3+},[15] along with the combination being targeted towards more advanced applications such as MRI contrasting agents,[16] luminescent phospholipid vesicles,[17] and oxygen sensing/$^1O_2$ generation.[18] Along with this it has been shown that when pyrene blue emission couples with Eu^{3+} or a combination of Eu^{3+} and Tb^{3+} emissions, in a MOF[19] or polymer network,[20] overall "white emission" is achievable. However, to the best of our knowledge, there has not been an investigation into discrete single

[a] Dr. A. T. O'Neil, J. Pope, Prof. J. A. Harrison, Prof. J. A. Kitchen
Chemistry, School of Natural Sciences
Massey University, Albany Campus
Auckland 0632 (New Zealand)
E-mail: j.kitchen@massey.ac.nz

Supporting information for this article is available on the WWW under https://doi.org/10.1002/ejic.202300358

Research Article
doi.org/10.1002/ejic.202300358

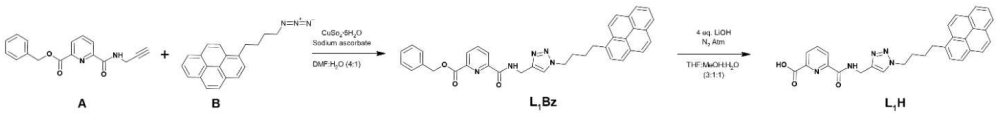

Scheme 1. Synthesis of ligand L_1H and intermediate L_1Bz from precursors **A** and **B**.

component self-assembling systems that utilize pyrene and Eu^{3+} to achieve white emission or fluorescent color-change sensing. Herein we report the synthesis, characterisation and complexation of L_1H with Eu^{3+} to form a discrete single component multi-emissive system. With the spatially distant secondary pyrene luminophore, the system's overall emission can be altered, resulting in close to pure white light as well as color changing oxygen sensing where the pyrene emission, but not the Eu^{3+}, is quenched by oxygen.

Results and Discussion

Ligand Synthesis and Characterization

Ligand 1 (L_1H) was prepared from 1-pyrenebutanol and our previously reported mono-alkyne (**A**) (Scheme 1).[11a] 1-Pyrenebutanol was converted into 1-(bromobutane)pyrene (**B**) by reaction with phosphorous tribromide before being transformed into 1-(azidobutane)pyrene (**C**) by heating in DMF with sodium azide. The benzyl protected ligand (L_1Bz) was prepared by CuAAC reaction of 1-(azidobutane)pyrene and **A**[11a] at 80 °C in 4:1 DMF:H_2O.[21] Removal of the benzyl protecting group was carried out using LiOH following reported procedures[11a] and resulted in L_1H as a brown solid in 85% yield. All compounds were characterized using ^{1}H-NMR, ^{13}C-NMR, FTIR and Mass Spectrometry. Successful formation of L_1H was confirmed by LRMS with a peak at 502.1 m/z corresponding to the deprotonated L_1^- species (calc. for $C_{30}H_{24}N_5O_3^-$, 502.5). ^{1}H-NMR also confirmed successful formation of L^1H, particularly when comparing spectra of the various intermediates (Figure S22). The appearance of a singlet resonance peak at ≈8 ppm assigned to the 1,2,3-triazole proton along with the expected resonances for other proton environments within L_1H gave clear evidence that formation was successful. Disappearance of the terminal alkyne proton at 4.1 ppm and CH_2-azide methylene at 3.5 ppm (shifting to 4.4 ppm as a CH_2-triazole signal) and the corresponding significant downfield shifts of methylene groups further confirmed 1,2,3-triazole formation. Deprotection of the benzyl ester protecting group was clearly indicated by the loss of benzyl aromatic protons (Bz, 7.2–7.5 ppm) and the CH_2–O linker (5.4 ppm). ^{13}C NMR also confirmed formation of L_1H with the correct number of carbon environments and appearance of 1,2,3-triazole ring signals [144.8 (C) and 123.5 (CH) ppm].

Single crystals suitable for X-ray diffraction of L_1Bz were grown by slow evaporation and the low temperature (123 K) molecular structure determined (Figure S15). L_1Bz crystallized in the monoclinic space group $P2_1/c$ and contained two crystallographically independent molecules of L_1Bz in the asymmetric unit. There are four water molecules also present within the asymmetric unit, however some were unable to be refined satisfactorily and were treated with the smbtx solvent mask routine in Olex2.[22] The molecular structure shows the expected connectivity for L_1Bz. The pyrene unit features weak off-set, face-to-face pi-stacking between the neighboring molecules with a centroid-centroid distance of 3.963 Å (shift distance 2.154 Å, $\delta = 57.18°$ and $\Theta = 57.13°$). Solvent molecules are involved in hydrogen bonding interactions to the carbonyl oxygen atoms and amide NH group (see SI for full details).

With successful synthesis and characterization of L_1H, a photophysical characterization of the ligand was undertaken in MeOH. The absorption spectrum of L_1H is dominated by the pyrene moiety with the characteristic three major absorptions at 214–250 nm ($S_0 \rightarrow S_4$), 256–280 nm ($S_0 \rightarrow S_3$) and 303–356 nm ($S_0 \rightarrow S_2$), along with a very weak transition at 370 nm ($S_0 \rightarrow S_1$).[13] Absorptions related to the pyridyl and 1,2,3-triazole groups are likely masked by the pyrene signals. The emission spectrum of L_1H showed classic pyrene emission when excited into any of the three major absorption bands mentioned above, giving emission peaks at 378 nm, 397 nm, and 419 nm. Under UV irradiation ($\lambda_{ex} = 355$ nm) L_1H emits blue light as a solid and as a 0.01 mM solution (Figure 1). Fluorescence quantum yields of the pyrene centered emission were determined by the dilute comparison method[23] against quinine sulfate in 0.5 M H_2SO_4. Φ_f was found to be relatively weak ($\Phi_f = 2.6\%$).

Coordination of L_1H with Eu^{3+} and La^{3+}

Initial studies into the coordination ability of L_1H involved spectroscopic titrations in MeOH where incremental amounts of Eu^{3+} were added to L_1^- and changes to the electronic spectra monitored. With the absorption spectrum of L_1H dominated by

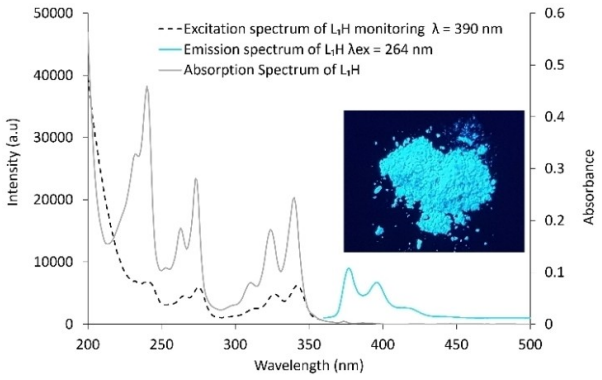

Figure 1. Absorption, excitation, and emission spectra of L_1H.

Research Article
doi.org/10.1002/ejic.202300358

the pyrene transitions, titrations with $Eu(CF_3SO_3)\cdot 6H_2O$ showed only small changes upon the addition of 0–4 equivalents of Eu^{3+} (Figures S26–S27). The largest change occurred between 280 and 290 nm where 0–0.35 equivalents and resulted in a red shift and small hyperchromic effect. Further addition did not result in any significant red shift or blue shift and the intensity change plateaued indicating formation of $Eu(\mathbf{L_1})_3$. Fluorescence titrations showed significant changes on addition of 0–0.35 equivalents of Eu^{3+} (Figures S28–S29). Most obvious was the increase in Eu^{3+} centered emission which increased up to 0.35 equiv. before slightly decreasing, indicating initial formation of the $Eu(\mathbf{L_1})_3$ species before disassembly into the less emissive $Eu(\mathbf{L_1})_2$ and $Eu(\mathbf{L_1})$ – as has been observed in similar systems.[11a,21] Pyrene emission also changes on addition of 0–0.35 equiv. Eu^{3+} with monomer emission at 395 nm decreasing while excimer emission at 475 nm increases, likely associated with intramolecular π-π stacking between pyrene units within the $Eu(\mathbf{L_1})_3$. On further addition a slight increase in monomer emission and slight decrease in excimer emission was observed. Fitting the fluorescence titration data (570–720 nm) using ReactLab™ Equilibria[24] gave speciation over the course of the titration and showed formation of $Eu(\mathbf{L_1})_3$ at 0.3 equivalents (51%), followed by $Eu(\mathbf{L_1})_2$ at 0.45 equivalents (57%) and finally $Eu(\mathbf{L_1})$ at 0.7 equivalents (59%) (Figure S30).

With the ability to form the 1:3 complex confirmed from spectroscopic titrations, bulk solids of $Eu(\mathbf{L_1})_3$ and $La(\mathbf{L_1})_3$ were prepared by reacting 3 equivalents of $\mathbf{L_1H}$ with 3 equivalents of triethylamine and 1 equivalent of $Eu(CF_3SO_3)_3\cdot 6H_2O$ or $La(CF_3SO_3)_3\cdot 9H_2O$ in DCE:EtOH (1:1). The reaction solutions were subjected to vapour diffusion of diethyl ether yielding pale brown powders (70% and 72% respectively). Mass spectrometry confirmed the formation of the desired complexes with *m/z* values of 1682.52 for $[Eu(\mathbf{L_1})_3+Na]^+$ (calc. for $(C_{90}H_{72}N_{15}O_9EuNa)^+$, 1682.58) and 1669.65 for $[La(\mathbf{L_1})_3+Na]^+$ (calc. for $(C_{90}H_{72}N_{15}O_9LaNa)^+$, 1669.52). FTIR confirmed coordination to the lanthanide with shifts observed in both the COOH and CONH carbonyls (see SI for details). ^{1}H NMR of $La(\mathbf{L_1})_3$ was run in DMSO-d_6 (Figure S37) and showed evidence of La^{3+} coordination with spectral broadening and downfield shifts. For example an approx. 0.7 ppm downfield shift was experienced by the amide (NH) indicative of La^{3+} binding in the NO_2 pocket.[25] Shifts to pyridyl protons are the most telling when analyzing these systems and whilst shifts in the pyridyl region are evident, they are masked by the pyrene signals. Despite this, there are clear changes to the pyridyl protons indicating binding. Although the exact species formation is not evident from ^{1}H-NMR, the NMR and IR shifts are indicative of Ln^{3+} coordination in the NO_2 pocket akin to previous systems[11a,21,25]

$Eu(\mathbf{L_1})_3$ Complex Photophysical Characterization

With successful formation of complexes determined, a detailed photophysical study of $Eu(\mathbf{L_1})_3$ was carried out in MeOH (0.01 mM). The UV/Vis spectrum of $Eu(\mathbf{L_1})_3$ (Figure S32) retained the dominant pyrene-based absorptions, including the red shift between 280–290 nm as seen in titration data, indicating complexation. When excited within the pyridyl associated absorption region (220–290 nm) the fluorescent spectrum of $Eu(\mathbf{L_1})_3$ showed effective population of the $^5D_0$ excited state of Eu^{3+} and the subsequent deactivation to the ^7F_J (J = 0–4) states. This resulted in sharp emission bands centered at λ = 594 nm ($^5D_0\rightarrow{}^7F_1$), 616 nm ($^5D_0\rightarrow{}^7F_2$), 651 nm ($^5D_0\rightarrow{}^7F_3$), 697 nm ($^5D_0\rightarrow{}^7F_4$) and 581 nm ($^5D_0\rightarrow{}^7F_0$), the latter signal indicative of the overall symmetry potentially being C_3 (Figure 2).[26] Excitation at 220–290 nm also resulted in pyrene centered emission with both monomer emission at 390 nm and excimer emission at 480 nm. The appearance of excimer emission in $Eu(\mathbf{L_1})_3$ is a result of intramolecular interactions between the pyrene motifs on the three ligands, as previously observed during self-assembly titrations. Excitation beyond 300 nm (up to 380 nm) resulted only in pyrene-centered emission, with no Eu^{3+} emission. The excitation spectrum showed Eu^{3+} centered emission (616 nm) originating between 220–290 nm (the

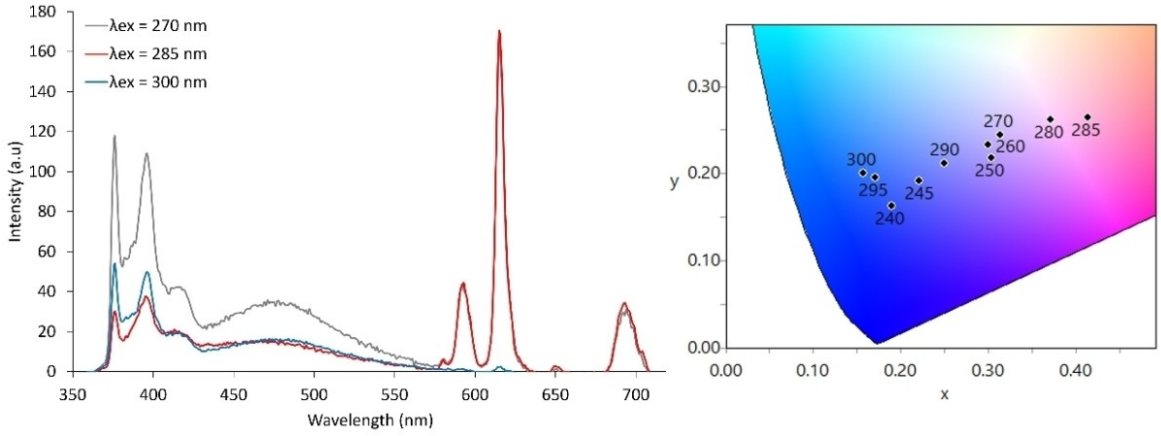

Figure 2. (Left) Fluorescence spectra of $Eu(\mathbf{L_1})_3$ at low concentration (0.01 mM, MeOH), showing change in Eu^{3+} and Pyrene centered emission at different excitation wavelengths. (Right) Corresponding CIE 1931 chromaticity diagram with different overall colors capable of the $Eu(\mathbf{L_1})_3$ solution (0.01 mM MeOH), when excitation wavelength changes from 240 nm to 300 nm. Calculated CIE coordinates: 240 nm x,y = 0.19, 0.16; 245 nm x,y = 0.22, 0.19; 250 nm x,y = 0.30, 0.22; 270 nm x,y = 0.31, 0.24; 280 nm x,y = 0.37, 0.26; 285 nm x,y = 0.41, 0.27; 290 nm x,y = 0.25, 0.29 and 300 nm x,y = 0.16, 0.20.

Research Article
doi.org/10.1002/ejic.202300358

absorption range of the central pyridyl motif). The lack of Eu^{3+} centered emission beyond 290 nm suggests the pyrene motif is not capable of populating the Eu^{3+} excited states (unlike in other pyrene systems in literature)[14] indicating the pyrene motif is too distant from the Eu^{3+} for energy transfer to occur. When pyrene centered emission (375 nm, 400 nm, and 480 nm) was monitored, the excitation spectrum ranged 220 to 380 nm with a spectral shape similar to the absorption spectrum of pyrene. The total quantum yield (Φ^{L}_{Ln}) of Eu^{3+} emission was measured using the dilute comparison method[23] giving a low value of 0.19%, likely from the strong pyrene absorbance overlapping the pyridyl antenna absorption, resulting in significantly weaker emission. The quantum yield for the pyrene emission was measured for both $Eu(\mathbf{L_1})_3$ (1.5%) and $La(\mathbf{L_1})_3$ (1.7%) and was found to be weaker than in the free ligand (2.6%), likely associated with enhanced excimer formation in the complexes. With two chromophores present within $Eu(\mathbf{L_1})_3$ we investigated tuning the overall emission profile by altering the excitation wavelength and populating excited states of Eu^{3+} and pyrene to differing degrees, given that the absorption spectrum showed overlapped pyrene and pyridyl absorbances. In the solid state when $Eu(\mathbf{L_1})_3$ is irradiated with longwave UV (λ_{ex} = 355 nm) the sample appears blue, whilst under shortwave (λ_{ex} = 257 nm) it appears white (Figure 3). At shortwave both chromophores emit with the overall combination appearing "white", whilst at longwave emission is dominated by pyrene resulting in the blue appearance. This was further demonstrated in 0.01 mM MeOH solution, where it was observed that the overall emission remains blue (see Figure 2 for CIE coordinates) when the excitation wavelengths are greater than 290 nm and less than 250 nm where pyrene centered emission dominates. Excitation wavelengths between 250 nm and 290 nm resulted in Eu^{3+} centered emission alongside pyrene emission resulting in the overall emission moving towards the "white emission" region (λ_{ex} = 270 nm CIE coordinates, x,y = 0.31, 0.24).[7a,27] Maximum Eu^{3+} centered emission is observed at λ_{ex} = 285 nm resulting in a pale red emission (CIE coordinates, x,y = 0.41, 0.27).

These results showed that the overall emission of $Eu(\mathbf{L_1})_3$ is color-tunable in both solution and solid-state, with overall emission ranging from blue to red. Additionally, $Eu(\mathbf{L_1})_3$ resulted in emission within the white region (pure white-emission is considered to have CIE coordinates of x,y = 0.333, 0.333).[7a,28] To move closer to pure white-emission the solution concentration was increased to 5 mM to favor aggregation induced intermolecular excimer formation,[29] which has previously been used in similar single component systems to improve upon white emission.[7d] As a result $Eu(\mathbf{L_1})_3$ overall emission is dominated by excimer emission at 490 nm, with little sign of pyrene monomer emission (Figure 4). This causes the color-tunable range of $Eu(\mathbf{L_1})_3$ to reduce, such that excitation above 290 nm and below 250 nm results in similar light blue emission and does not achieve the deeper blue as previously observed. However, because of the dominant excimer emission in combination with the Eu^{3+} emission, the overall emission largely remains within the white region. At λ_{ex} of 270 nm and 280 nm the overall emission is near "pure white" with x,y = 0.317, 0.333 and x,y = 0.329, 0.324 respectively.

Finally, the single component dual emissive $Eu(\mathbf{L_1})_3$ was investigated for its potential as an oxygen sensor. Pyrene emission is known to be quenched by the presence of oxygen.[30] To test the ability of oxygen to quench $Eu(\mathbf{L_1})_3$, a 0.01 mM solution in MeOH:DCM (1:1) was excited at 283 nm

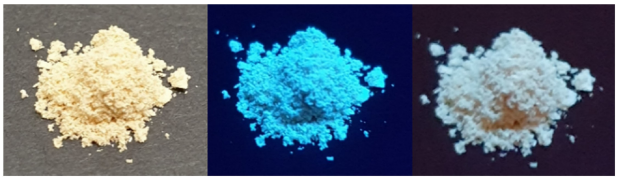

Figure 3. Solid powder of $Eu(\mathbf{L_1})_3$ under ambient light, longwave irradiation (λ_{ex} = 365 nm), and shortwave irradiation (λ_{ex} = 254 nm), from left to right.

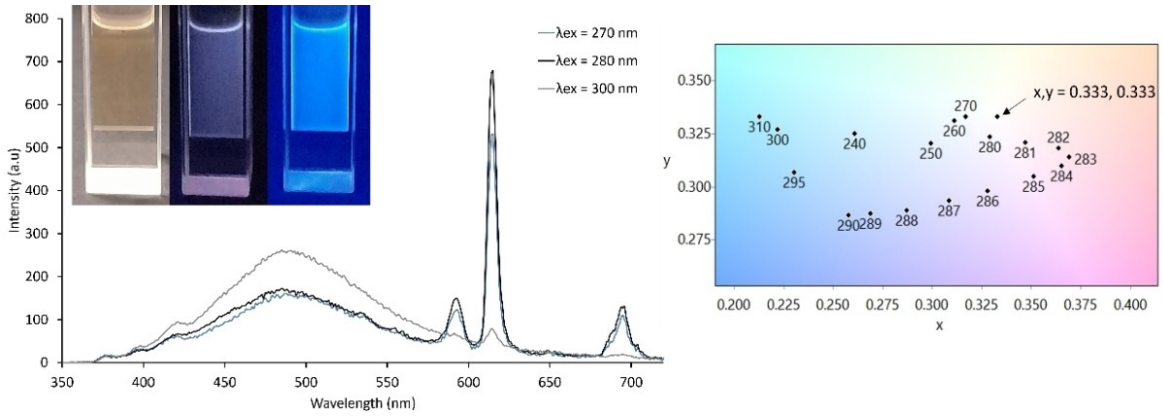

Figure 4. (Left) Fluorescence spectra of $Eu(\mathbf{L_1})_3$ at higher concentration (5 mM, MeOH) showing change in Eu^{3+} and Pyrene centered emission at different excitation wavelengths. Insert: image of $Eu(\mathbf{L_1})_3$ solution under ambient light, longwave irradiation (λ_{ex} = 365 nm), and shortwave irradiation (λ_{ex} = 254 nm), from left to right. (Right) Corresponding CIE 1931 chromaticity diagram with different overall colors capable by $Eu(\mathbf{L_1})_3$ in solution (5 mM, MeOH), when excitation wavelength changes from 240 nm to 310 nm. Calculated CIE coordinates: 240 nm x,y = 0.26, 0.33; 250 nm x,y = 0.30, 0.32; 270 nm x,y = 0.32, 0.33; 280 nm x,y = 0.33, 0.32; 281 nm x,y = 0.35, 0.32; 282 nm x,y = 0.36, 0.32; 283 nm x,y = 0.37, 0.31; 284 nm x,y = 0.36, 0.31; 285 nm x,y = 0.32, 0.30; 286 nm x,y = 0.33, 0.30; 287 nm x,y = 0.31, 0.29; 288 nm x,y = 0.29, 0.29; 282 nm x,y = 0.27, 0.28; 290 nm x,y = 0.26, 0.29; 295 nm x,y = 0.23, 0.30; 300 nm x,y = 0.22, 0.33; and 340 nm x,y = 0.21, 0.32.

Research Article
doi.org/10.1002/ejic.202300358

(giving both pyrene and Eu^{3+} centered emission) and oxygen gas bubbled through for 1 minute. This resulted in a significant decrease in pyrene centered emission while the Eu^{3+} centered emission remained relatively unchanged (as expected from the pyrene not acting as an antenna for the Eu^{3+} in this system). As a result, the overall emission switches from white to light red (Figure 5). The solution was then deoxygenated by bubbling nitrogen gas through the solution for 1 minute, which resulted in an increase in pyrene emission and once again Eu^{3+} centered emission remained relatively unchanged. Interestingly, the overall emission switched from light red to blue with the original white emission not recovered, likely through more oxygen being removed through N_2 flushing than was in the original solution. Reoxygenating was again carried out resulting in the solution switching back to the overall emission of red. This demonstrated that Eu($\mathbf{L_1}$)$_3$ can act as an oxygen sensor, with a color switching from blue to red and vice versa dependent on the oxygen concentration present. Furthermore, with only one of the two emissive chromophores changing in the presence of oxygen, Eu($\mathbf{L_1}$)$_3$ has the potential to act as a ratiometric sensor with a self-calibrating Eu^{3+} signal.[1a,31] The oxygen sensing is reversible when cycling between oxygen and nitrogen. Furthermore, it recovers to the original emission profile approximately 20–30 minutes post addition of oxygen or nitrogen (see Figures S39–S42).

Conclusions

In summary, a simple pyrene-containing PDC based-ligand ($\mathbf{L_1H}$) has been synthesised and complexed with Eu^{3+} and La^{3+}. Eu($\mathbf{L_1}$)$_3$ was shown to be a rare example of a single component dual emissive lanthanide complex exhibiting both pyrene and Eu^{3+} emission. The complex exhibits emission color tuning where the overall emission profile is dependent on excitation wavelength with a color-profile that includes white-emission. Furthermore the single component dual emissive system was found to be oxygen sensitive with pyrene emission quenching upon introduction of oxygen into a solution of Eu($\mathbf{L_1}$)$_3$ while the Eu^{3+} emission remained relatively unchanged. Tunable single component white-emissive systems are uncommon[7a] and our approach has demonstrated the potential for such systems to generate interesting optical and sensing materials. The simplicity of our ligand design/synthesis means new chromophores can be easily incorporated. Further investigation into improved organic chromophore inclusion is currently underway.

Experimental Section

Materials and Methods: All reagents, solvents and starting materials were purchased from Sigma-Aldrich. NMR spectra were recorded using a Bruker Ultrashield 300, with chemical shifts recorded in parts per million (ppm). UV/Vis spectra were recorded on a Shimadzu UV-1800 using CH_2Cl_2 and MeOH solvent in a 3 mL quartz cuvette with a 1 cm path length. Steady state fluorescence measurements were recorded on a Shimadzu RF-6000 Spectro fluorophotometer, with a ZJB380 UV emission filter (300 nm) in CH_2Cl_2 and MeOH solvent in a capped 3.5 mL quartz cuvette with a 1 cm path length. Melting points were obtained on an Electrothermal IA9000 Series Melting Point Apparatus. Fourier-transform infrared spectra (FT-IR) of solids were recorded on a Bruker Alpha platinum-ATR. Mass spectrometry was carried out in HPLC grade solvents, using a Shimadzu LCMS-2020. Single crystal X-ray diffraction data were collected at 123 K on a Bruker D8 Venture equipped with a IμS DIAMOND microfocus Cu–Kα ($\lambda = 1.54178$) X-ray source with a PHOTON III detector. Unit cell parameters were refined against all data and an empirical absorption correction applied in APEX3. Structures were solved by direct methods using SHELXS-2013 and refined by SHELXL-2013[32] using Olex2,[22] Deposition Number 2206173 (for $\mathbf{L_1Bz}$) contains the supplementary crystallographic data for this paper. These data are provided free of charge by the joint Cambridge Crystallographic Data Centre and Fachinformationszentrum Karlsruhe Access Structures service. Commission Internationale de l'Elcairage (CIE) plots were generated in OSRAM LED ColorCalculator software.[33] Photophysical titration data was fitted with ReactLab™ Equilibria[24] for non-linear regression analysis. Quantum yield measurements were determined by the dilute comparison method[23] using relative standards Cs_3[Eu(dpa)$_3$]·$8H_2O$ and in a 0.1 M Tris–HCl buffer solution (pH ≈ 7.45) and quinine sulfate in 0.5 M H_2SO_4, with known quantum yields of $\Phi_{ref} = 24 \pm 2.5\%$ and $\Phi_{ref} = 54.6\%$ respectively. Cs_3[Eu(dpa)$_3$]·$8H_2O$ was used for Eu($\mathbf{L_1}$)$_3$ and quinine sulfate was used for pyrene emission.[34] Barrier slit widths remained the same between

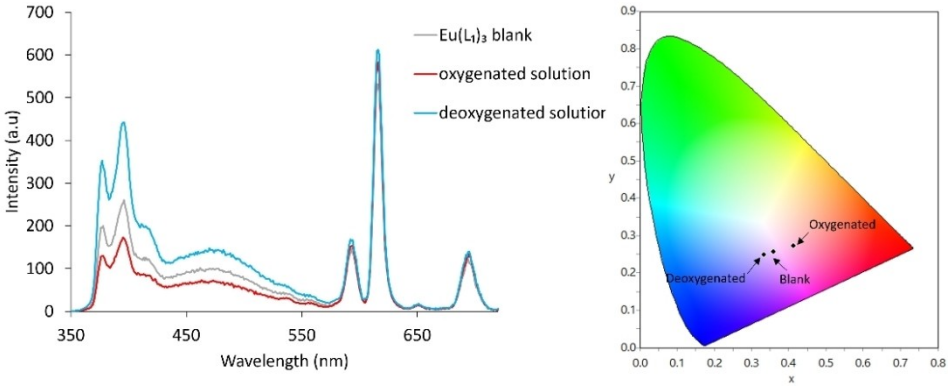

Figure 5. (Left) Fluorescence spectra of Eu($\mathbf{L_1}$)$_3$ solution, (0.01 mM, MeOH:DCM (1:1)) with and without oxygen – under standard conditions ("Blank") and after the solution has been oxygenated and deoxygenated. This resulted in significant changes to the pyrene emission whilst Eu^{3+} emission was less effected. (Right) Corresponding CIE 1931 chromaticity diagram of the Eu($\mathbf{L_1}$)$_3$ solution under different oxygenation conditions – showing overall color change from white (blank) to red (oxygenated) or blue (deoxygenated) dependent on the presence of oxygen

measurements for different compounds with either 1.5 or 3 nm excitation and emission widths. The excitation wavelength was the same for all measurements with 279 nm excitation wavelength being used for lanthanide standards/emissions and 366 nm for quinine sulfate/pyrene emissions. Lanthanide standards were initially cross calibrated to be within the range of error before being compared to lanthanide complexes. See supplementary information for further details. Safety Note: low molecular weight organic azides are potential explosives, and care must be taken during their handling; however, no issues were encountered here.

Synthesis of 1-(bromobutane)pyrene (B):[35] 1-Pyrenebutanol (0.5 g, 1.8 mmol) was dissolved in 20 mL of dry ethyl acetate, to which 0.5 mL of PBr_3 was added dropwise. This was left to stir at room temperature for 20 minutes, causing the solution to turn a pale yellow; the solution was then refluxed for 12 hours. Ice cold H_2O was then added dropwise to the solution while stirring until solution went cloudy; the solution was then stored at 4 °C for 24 hours, causing a fine white precipitate, which was then filtered giving **B** as an off-white solid (0.57 g, 92%). Melting point = 103 °C. LRMS *m/z* = 338.25 $[\mathbf{B}+H]^+$ (calc. for $C_{20}H_{18}Br^+$, 338.26) and *m/z* = 360.25 $[\mathbf{B}+Na]^+$ (calc. for $C_{20}H_{17}BrNa^+$, 360.24). NMR (300 MHz, $CDCl_3$, ppm), δ = 8.28 (d, J = 10.5 Hz, 1H, CH), 8.15 (m, 4H, pyrene–H), 8.03 (s, 2H, pyridine–H), 8.00 (t, 8.0 Hz, 1H, pyrene–H), 7.78 (d, J = 8.0 Hz, 1H, pyrene–H), 3.47 (t, J = 6.5 Hz, 2H, CH_2–Br) 4.10 (t, J = 7.0 Hz, 2H, CH_2–pyrene) 2.19 (m, 4H, CH_2–**CH_2**–**CH_2**–CH_2); ^{13}C NMR (75 MHz, $CDCl_3$, ppm): δ = 136.1 (C), 131.4 (C), 130.9 (C), 129.9 (C), 128.6 (C), 127.5 (CH), 127.4 (CH), 127.2 (CH), 126.7 (CH), 126.7 (CH), 125.9 (CH), 125.1 (C), 125.0 (C), 124.9 (CH), 124.8 (CH), 124.8 (CH), 33.63 (CH_2), 32.6 (CH_2), 30.2 (CH_2). FTIR (cm^{-1}) 2948, 1695, 1658, 1586, 1511, 1440, 1382, 1359, 1336, 1242, 1211, 1168, 1138, 1084, 1028, 1011, 887, 847, 800, 778, 740, 672, 620, 542, 483, 412.

Synthesis of 1-(azidobutane)pyrene (C): B (0.8 g, 2.3 mmol) was combined with NaN_3 (0.3 g, 4.6 mmol) in 20 mL of DMF and the colorless solution was heated at 80 °C for 24 hours. The solution was allowed to cool, and 20 mL of H_2O was added to the pale pink solution causing a white precipitate to form, which was redissolved into 30 mL of ethyl acetate. The organic layer was separated and then washed with 2×20 mL H_2O, then brine, and then dried with $MgSO_4$ before solvent was removed, yielding **C** as a pale pink solid (0.6 g, 85%). ^1H NMR (300 MHz, $CDCl_3$, ppm), δ = 8.26 (d, J = 9.5 Hz, 1H, pyrene–H), 8.14 (m, 4H, pyrene–H), 8.03 (S, 2H, pyridine–H), 7.99 (t, J = 8.0 Hz, 1H, pyrene–H), 7.86 (d, J = 8.0 Hz 1H, pyrene–H), 3.36 (m, 4H, pyrene–CH_2, N_3–CH_2), 1.95 (m, 1H, CH_2) 1.79 (m, 2H, CH_2); ^{13}C NMR (75 MHz, $CDCl_3$, ppm): δ = 136.1 9 (C), 131.4 (C), 130.9 (C), 129.9 (C), 128.6 (C), 127.5 (CH), 127.3 (CH), 127.2 (CH), 126.7 (CH), 125.8 (CH), 125.1 (C), 125.0 (C), 124.9 (CH), 124.8 (CH), 127.7 (CH), 123.2 (CH), 51.4 (CH_2), 33.0 (CH_2), 28.9 (CH_2), 28.8 (CH_2). FTIR (cm^{-1}) 3040, 2966, 2938, 2924, 2862, 2352, 2202, 2089 (N_3), 1806, 1600, 1582, 1506, 1485, 1464, 1455, 1428, 1414, 1366, 1351, 1332, 1306, 1295, 1278, 1245, 1228, 1182, 1098, 1070, 1049, 1017, 970 892, 839, 816, 795, 777, 759, 747, 709, 679, 664, 607, 587, 552, 536, 517, 489, 434, 417.

Synthesis of N_2-((1-(1-butane)pyrene)-1H-1,2,3-triazol-4-yl)methyl)-O_6-((benzyloxy)carbonyl)pyridine-2-carboxamide-6-carboxylate (L_1Bz): A[11a] (0.41 g, 1.4 mmol) was combined with sodium ascorbate (0.22 g, 1.4 mmol), $CuSO_4 \cdot 5H_2O$ (0.14 g, 0.7 mmol) and **C** (0.50 g, 1.4 mmol) in 30 mL of DMF:H_2O (4:1). The solution was heated to 80 °C overnight, changing from a light yellow to a brown. Water was slowly added to the solution until a cloudy precipitate was formed, which was filtered and then washed with (0.1 M) NaOH:(0.5 M) EDTA solution yielding a brown crystalline solid. The solid was redissolved into 10 mL DCM:MeOH (1:1) and washed with 2×50 mL H_2O and evaporated yielding L_1Bz as a pale cream solid (0.36 g, 44%). Melting point = 97.5 °C. LRMS *m/z* = 594.10 $[L_1Bz+H]^+$ (calc. for $C_{37}H_{32}N_5O_3^+$, 594.68), *m/z* = 616.15 $[L_1Bz+Na]^+$ (calc. for $C_{37}H_{31}N_5O_3Na^+$, 616.66) and *m/z* = 632.15 $[L_1Bz+K]^+$ (calc. for $C_{37}H_{31}N_5O_3K^+$, 632.77). NMR (300 MHz, $CDCl_3$, ppm), δ = 8.68 (m, 1H, NH), 8.3 (dd, J = 8.0, 1.0 Hz, 1H, pyrene–H), 8.20–7.90 (m, 11H, pyridine–H and pyrene–H), 7.51 (s, 1H, triazole–H), 7.40 (m, 5H, benzene), 5.41 (s, 2H, CH_2–O), 4.72 (d, J = 6.0 Hz, 2H, CH_2–NH) 4.34 (t, J = 7.0, 2H, CH_2–N), 3.36 (t, J = 7.5 Hz, 2H, CH_2–pyrene), 2.03 (m, 2H, CH_2–CH_2–N), 1.89 (m, 2H, CH_2–CH_2–pyrene); ^{13}C NMR (75 MHz, $CDCl_3$, ppm): δ = 164.2 (C=O), 163.7 (C=O), 149.9 (CN), 146.6 (CN), 144.6 (C-t), 138.5 (CH), 131.4 (C), 130.8 (C), 130.0 (C), 128.7 (CH), 128.6 (CH), 128.6 (CH), 127.5 (CH), 127.5 (CH), 127.3 (CH), 126.8 (CH), 125.9 (CH), 125.4 (CH), 125.1 (C), 125.0 (CH), 124.8 (C), 124.8 (CH), 123.1 (CH), 122.4 (CH), 67.7 (CH_2), 50.3 (CH_2), 35.1 (CH_2), 32.7 (CH_2), 30.1 (CH_2), 28.5 (CH_2). FTIR (cm^{-1}) 3505, 3315, 3140, 3039, 2935, 2864, 1721, 1673, 1650, 1585, 1529, 1428, 1381, 1338, 1299, 1263, 1234, 1213, 1170, 1146, 1100, 1081, 1054, 1002, 985, 962, 938, 904, 843, 817, 783, 752, 730, 708, 691, 675, 650, 635, 585, 528, 488, 460, 428.

Synthesis of N_2-((1-(1-butane)pyrene)-1H-1,2,3-triazol-4-yl)methyl)pyridine-2-carboxamide-6-carboxylate (L_1H): L_1Bz (0.38 g, 0.64 mmol) was combined with LiOH (0.061 g, 2.56 mmol) in 20 mL of THF:MeOH:H_2O (3:1:1), which was stirred overnight under a nitrogen atmosphere, where the solid slowly dissolved into a light yellow solution. The solvent was then removed until a residue remained. 1 M HCl was added to the solution causing an off-white precipitate to form, which was filtered and washed with water, yielding **L_1H** as a brown solid (0.27 g, 85%). Melting point = 115.9 °C. LRMS *m/z* = 502.1 $[\mathbf{L_1H}-H]^-$ (calc. for $C_{30}H_{24}N_5O_3^-$, 502.54).^1H NMR (300 MHz, DMSO-d_6, ppm), δ = 9.74 (t, J = 6.0 Hz, 1H, NH), 8.34–7.91 (m, 13H, pyrene–H, 1,2,3-triazole–H and pyridine–H), 4.61 (d, J = 6.0 Hz, 2H, CH_2–NH), 4.43 (t, J = 6.0 Hz, 2H, CH_2–N), 3.35 (t, J = 7.5 Hz, 2H, CH_2–pyrene–H), 1.98 (m, 2H, **CH_2**–CH_2–N), 1.74 (m, 2H, **CH_2**–CH_2–pyrene), ^{13}C NMR (75 MHz, DMSO-d_6, ppm): δ = 165.2 (C=O), 163.3 (C=O), 149.6 (CN), 146.5 (CN), 144.9 (C-t), 140.4 (CH), 137.0 (C), 131.4 (C), 129.7 (C), 128.5 (C), 127.9 (C), 127.7 (CH), 127.1 (CH), 127.0 (CH), 126.6 (CH), 125.9 (CH), 125.4 (CH), 125.2 (CH), 124.7 (C), 124.6 (C), 123.9 (C), 123.5 (CH-t), 49.5 (CH_2), 34.9 (CH_2), 32.3 (CH_2), 30.2 (CH_2), 34.3 (CH_2), 28.8 (CH_2). FTIR (ATR, cm^{-1}) 3218, 3039, 2934, 2862, 2451, 2330, 2094, 1890, 1740, 1671, 1602, 1585, 1526, 1454, 1432, 1339, 1246, 1181, 1141, 1102, 1074, 1001, 842, 742, 721, 708, 678, 643, 618, 556, 505, 423.

General procedure for complexation of L_1H with lanthanide ions

L_1H was dissolved in 5 mL of DCE:EtOH (1:1), and 1 equivalent of triethylamine was added followed by 0.33 equivalents of selected lanthanide triflate salt (from a stock solution in MeOH), yielding a clear brown solution. The solution was refluxed for 30 minutes and then subjected to vapour diffusion of diethyl ether at room temperature until precipitation or film formation occurred.

Synthesis of Eu(L_1)$_3$: L_1H (30 mg, 0.063 mmol) was combined with 1 equivalent of triethylamine (9 mL) in 5 mL of DCE:EtOH (1:1). To this was added a methanolic solution of $Eu(CF_3SO_3)_3 \cdot 6H_2O$ (15 mg, 0.021 mmol). The resulting clear brown solution was refluxed for 30 minutes. The pale brown solution was cooled and then subjected to vapour diffusion of diethyl either, yielding a pale brown film. The solution was decanted, and the brown film collected, yielding Eu($\mathbf{L_1}$)$_3$ as a pale brown solid (23 g, 70%). LRMS *m/z* = 852.80 $[Eu(\mathbf{L_1})_3+2Na]^{2+}$ (calc. for $(C_{90}H_{72}N_{15}O_9EuNa_2)^{2+}$, 852.90) and *m/z* = 1682.35 $[Eu(\mathbf{1})_3+Na]^+$ (calc. for $(C_{90}H_{72}N_{15}O_9EuNa)^+$, 1682.58). FTIR ($cm^{-1}$) 3268, 3040, 2943, 2342, 2330, 1632, 1588, 1564, 1463, 1431, 1390, 1278, 1240, 1223, 1157, 1084, 1060, 1028, 893, 843, 818, 800, 757, 722, 682, 660, 636, 573, 516, 411.

Research Article
doi.org/10.1002/ejic.202300358

Synthesis of $La(L_1)_3$: L_1H (12.5 mg, 0.026 mmol) was combined with $La(CF_3SO_3)_3 \cdot 9H_2O$ (6.4 mg, 0.009 mmol) and 1 equivalent of triethylamine (3.5 mL) in 5 mL of DCE:EtOH (1:1). The resulting clear brown solution was refluxed for 30 minutes. The pale brown solution was then subjected to vapor diffusion of diethyl either, yielding a brown film. The solution was decanted, and the pale brown film collected, yielding $La(\mathbf{L_1})_3$ as a pale brown solid (10 mg, 72%). LRMS $m/z =$ 1669.65 $[La(\mathbf{L_1})_3 + Na]^+$ (calc. for $(C_{90}H_{72}N_{15}O_9LaNa)^+$, 1669.52). FTIR ($cm^{-1}$) 3253, 3040, 2942, 1633, 1588, 1566, 1464, 1432, 1391, 1279, 1241, 1224, 1158, 1084, 1048, 1029, 892, 843, 818, 800, 757, 722, 682, 660, 636, 573, 516, 414.

Supporting Information

The authors have cited additional references within the Supporting Information.[36]

Acknowledgements

Open Access publishing facilitated by Massey University, as part of the Wiley - Massey University agreement via the Council of Australian University Librarians.

Conflict of Interests

The authors declare no conflict of interest.

Data Availability Statement

The data that support the findings of this study are available in the supplementary material of this article.

Keywords: lanthanides · luminescence · pyrene · sensing · supramolecular chemistry

[1] a) Y. Feng, J. Cheng, L. Zhou, X. Zhou, H. Xiang, *Analyst* **2012**, *137*, 4885–4901; b) S. González-Carrero, M. de la Guardia, R. E. Galian, J. Pérez-Prieto, *ChemistryOpen* **2014**, *3*, 199–205.
[2] a) Y. Zhou, B. Yan, *J. Mater. Chem. C* **2015**, *3*, 9353–9358; b) Y. G. Galyametdinov, A. S. Krupin, A. A. Knyazev, *Inorganics* **2022**, *10*, 94.
[3] a) T. Sun, Y. Gao, Y. Du, L. Zhou, X. Chen, *Front. Chem.* **2021**, *8*; b) S. E. Plush, T. Gunnlaugsson, *Dalton Trans.* **2008**, 3801–3804.
[4] a) J. Wang, Y. Suffren, C. Daiguebonne, S. Freslon, K. Bernot, G. Calvez, L. Le Pollès, C. Roiland, O. Guillou, *Inorg. Chem.* **2019**, *58*, 2659–2668; b) H. J. Yu, X. L. Zhou, X. Dai, F. F. Shen, Q. Zhou, Y. M. Zhang, X. Xu, Y. Liu, *Chem. Sci.* **2022**, *13*, 8187–8192.
[5] M. A. Hernández-Rodríguez, C. D. S. Brites, G. Antorrena, R. Piñol, R. Cases, L. Pérez-García, M. Rodrigues, J. A. Plaza, N. Torras, I. Díez, A. Millán, L. D. Carlos, *Adv. Opt. Mater.* **2020**, *8*, 2000312.
[6] D. Kim, K. Jeong, J. E. Kwon, H. Park, S. Lee, S. Kim, S. Y. Park, *Nat. Commun.* **2019**, *10*, 3089.
[7] a) S. SeethaLekshmi, A. R. Ramya, M. L. P. Reddy, S. Varughese, *J. Photochem. Photobiol. C* **2017**, *33*, 109–131; b) J. Zhang, H. Li, P. Chen, W. Sun, T. Gao, P. Yan, *J. Mater. Chem. C* **2015**, *3*, 1799–1806; c) O. Kotova, S. Comby, C. Lincheneau, T. Gunnlaugsson, *Chem. Sci.* **2017**, *8*, 3419–3426; d) A. H. Shelton, I. V. Sazanovich, J. A. Weinstein, M. D. Ward, *Chem. Commun.* **2012**, *48*, 2749–2751; e) R. Boddula, J. Tagare, K. Singh, S. Vaidyanathan, *Mater. Chem. Front.* **2021**, *5*, 3159–3175; f) R. Shi, L. Yu, Y. Tian, X. Wang, Z. Sun, B. Qi, F. Luo, *Mater. Chem. Phys.* **2022**, *280*, 125806.
[8] N. A. Kukhta, M. R. Bryce, *Mater. Horiz.* **2021**, *8*, 33–55.
[9] a) K. Miyata, Y. Konno, T. Nakanishi, A. Kobayashi, M. Kato, K. Fushimi, Y. Hasegawa, *Angew. Chem. Int. Ed.* **2013**, *52*, 6413–6416; b) S. Wang, B. Sun, Z. Su, G. Hong, X. Li, Y. Liu, Q. Pan, J. Sun, *Inorg. Chem. Front.* **2022**, *9*, 3259–3266; c) X. Niu, M. Wang, M. Zhang, R. Cao, Z. Liu, F. Hao, L. Sheng, H. Xu, *Inorg. Front. Chem.* **2022**, *9*, 4582–4593; d) X. Zhai, P. Feng, N. Song, G. Zhao, Q. Liu, L. Liu, M. Tang, Y. Tang, *Inorg. Chem. Front.* **2022**, *9*, 1406–1415.
[10] S. V. Eliseeva, J.-C. G. Bünzli, *Chem. Soc. Rev.* **2010**, *39*, 189–227.
[11] a) A. T. O'Neil, J. A. Harrison, J. A. Kitchen, *Chem. Commun.* **2021**, *57*, 8067–8070; b) J. A. Kitchen, D. E. Barry, L. Mercs, M. Albrecht, R. D. Peacock, T. Gunnlaugsson, *Angew. Chem. Int. Ed.* **2012**, *51*, 704–708.
[12] Y. Li, D. Ji, J. Liu, Y. Yao, X. Fu, W. Zhu, C. Xu, H. Dong, J. Li, W. Hu, *Sci. Rep.* **2015**, *5*, 13195.
[13] A. G. Crawford, A. D. Dwyer, Z. Liu, A. Steffen, A. Beeby, L.-O. Pålsson, D. J. Tozer, T. B. Marder, *J. Am. Chem. Soc.* **2011**, *133*, 13349–13362.
[14] a) J. S. Sohna, F. Fages, *Tetrahedron Lett.* **1997**, *38*, 1381–1384; b) S. Bhowmik, S. Banerjee, U. Maitra, *Chem. Commun.* **2010**, *46*, 8642–8644.
[15] a) S. J. A. Pope, *Polyhedron* **2007**, *26*, 4818–4824; b) T. M. George, S. Varughese, M. L. P. Reddy, *RSC Adv.* **2016**, *6*, 69509–69520; c) S. Faulkner, M.-C. Carrié, S. J. A. Pope, J. Squire, A. Beeby, P. G. Sammes, *Dalton Trans.* **2004**, 1405–1409.
[16] M. F. Ferreira, G. Pereira, A. F. Martins, C. I. O. Martins, M. I. M. Prata, S. Petoud, E. Toth, P. M. T. Ferreira, J. A. Martins, C. F. G. C. Geraldes, *Dalton Trans.* **2014**, *43*, 3162–3173.
[17] M. Poznik, U. Maitra, B. König, *Org. Biomol. Chem.* **2015**, *13*, 9789–9792.
[18] a) R. Hueting, M. Tropiano, S. Faulkner, *RSC Adv.* **2014**, *4*, 44162–44165; b) A. Watkis, R. Hueting, T. J. Sørensen, M. Tropiano, S. Faulkner, *Chem. Commun.* **2015**, *51*, 15633–15636; c) Y. Hasegawa, T. Matsui, Y. Kitagawa, T. Nakanishi, T. Seki, H. Ito, Y. Nakasaka, T. Masuda, K. Fushimi, *Eur. J. Chem.* **2019**, *25*, 12308–12315.
[19] a) J. Park, M. Oh, *CrystEngComm* **2016**, *18*, 8372–8376; b) J. X. Li, Q. L. Guan, Y. Wang, Z. X. You, Y. H. Xing, F. Y. Bai, L. X. Sun, *New J. Chem.* **2020**, *44*, 1446–1454.
[20] P. Kumar, S. Soumya, E. Prasad, *ACS Appl. Mater. Interfaces* **2016**, *8*, 8068–8075.
[21] A. T. O'Neil, N. Zhang, J. A. Harrison, S. M. Goldup, J. A. Kitchen, *Supramol. Chem.* **2021**, *33*, 160–173.
[22] O. V. Dolomanov, L. J. Bourhis, R. J. Gildea, J. A. K. Howard, H. Puschmann, *J. Appl. Crystallogr.* **2009**, *42*, 339–341.
[23] G. A. Crosby, J. N. Demas, *J. Phys. Chem. A* **1971**, *75*, 991–1024.
[24] *ReactLab™ EQUILIBRIA (1.1)*, *Jplus Consulting Multivariate Analytical Technologies*, *Kilaben Bay*, *Australia*, *2022*.
[25] O. Kotova, S. Blasco, B. Twamley, J. O'Brien, R. D. Peacock, J. A. Kitchen, M. Martínez-Calvo, T. Gunnlaugsson, *Chem. Sci.* **2015**, *6*, 457–471.
[26] K. Binnemans, *Coord. Chem. Rev.* **2015**, *295*, 1–45.
[27] D. N. Anwar, A. Srivastava, *IEEE Access* **2020**, *8*, 159609–159621.
[28] Z. Zhang, Y.-N. He, L. Liu, X.-Q. Lü, X.-J. Zhu, W.-K. Wong, M. Pan, C.-Y. Su, *Chem. Commun.* **2016**, *52*, 3713–3716.
[29] A. S. Abd-El-Aziz, A. A. Abdelghani, B. D. Wagner, E. M. Abdelrehim, *Polym. Chem.* **2016**, *7*, 3277–3299.
[30] a) P. L. Chong, T. E. Thompson, *Biophys. J.* **1985**, *47*, 613–621; b) S. A. Ruetten, J. K. Thomas, *J. Phys. Chem. B* **1999**, *103*, 1278–1286.
[31] a) A. P. Demchenko, *Lab Chip* **2005**, *5*, 1210–1223; b) M. Amelia, A. Lavie-Cambot, N. D. McClenaghan, A. Credi, *Chem. Commun.* **2011**, *47*, 325–327.
[32] G. Sheldrick, *Acta Crystallogr. Sect. A* **2008**, *64*, 112–122.
[33] *LED ColorCalculator (7.77)*, *OSRAM SYLVANIA Inc.*, *2022*.
[34] a) A. M. Brouwer, *Pure Appl. Chem.* **2011**, *83*, 2213–2228; b) A. S. Chauvin, F. Gumy, D. Imbert, J. C. G. Bünzli, *Spectrosc. Lett.* **2004**, *37*, 517–532; c) A. S. Chauvin, F. Gumy, D. Imbert, J. C. G. Bünzli, *Spectrosc. Lett.* **2007**, *40*, 193–193.
[35] U. H. Sk, S. Bhattacharya, *Environ. Toxicol. Pharmacol.* **2006**, *22*, 298–308.
[36] G. A. Crosby, J. N. Demas, *J. Phys. Chem. A* **1971**, *75*, 991–1024.

Manuscript received: June 9, 2023
Revised manuscript received: July 27, 2023
Accepted manuscript online: August 14, 2023
Version of record online: August 31, 2023